

Supporting information

Tuning CuZn interfaces in metal-organic framework-derived electrocatalysts for enhancement of CO₂ conversion to C₂ products

*Saranya Juntrapirom,^a Jirapat Santatiwongchai,^a Athis Watwiangkham,^b Suwit Suthirakun,^b Teera
Butburee,^a Kajornsak Faungnawakij,^a Pongkarn Chakthranont,^{*a} Pussana Hirunsit^{*a} and Bunyarat
Rungtaweeveranit^{*a}*

^a National Nanotechnology Center (NANOTEC), National Science and Technology Development Agency
(NSTDA), Pathum Thani 12120, Thailand

^b School of Chemistry, Institute of Science, Suranaree University of Technology, Nakhon Ratchasima 30000,
Thailand

E-mail: pongkarn.cha@nanotec.or.th, pussana@nanotec.or.th, bunyarat.run@nanotec.or.th

Section S1: Synthesis and characterizations of $\text{Cu}_x\text{Zn}_{100-x}\text{-MOF-74}$ and $\text{Cu}_x\text{Zn}_{100-x}\text{-C}$

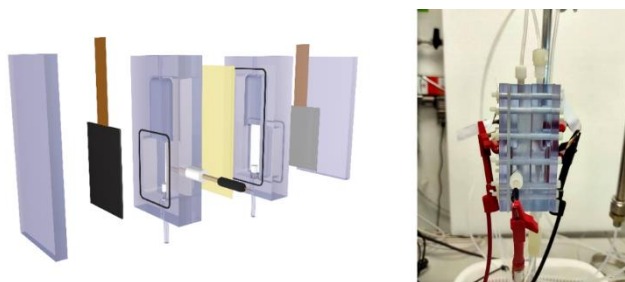


Fig. S1 H-type cell for the electrochemical CO_2 reduction reaction.

Table S1 Chemicals and their content for the synthesis of $\text{Cu}_x\text{Zn}_{100-x}\text{-MOF-74}$.

Sample	H_2DOBDC linker (g)	$\text{Cu}(\text{OAc})_2 \cdot \text{H}_2\text{O}$ (g)	$\text{Zn}(\text{OAc})_2 \cdot 2\text{H}_2\text{O}$ (g)	Cu/Zn ratio
Cu-MOF-74	0.2	0.40	0	-
$\text{Cu}_{90}\text{Zn}_{10}\text{-MOF-74}$	0.2	0.36	0.44	9:1
$\text{Cu}_{75}\text{Zn}_{25}\text{-MOF-74}$	0.2	0.30	0.22	3:1
$\text{Cu}_{50}\text{Zn}_{50}\text{-MOF-74}$	0.2	0.20	0.11	1:1
Zn-MOF-74	0.2	0	0.044	-

Table S2 Calculated lattice parameters of Cu(111) in $\text{Cu}_x\text{Zn}_{100-x}\text{-C}$ calculated from the PXRD results.

Sample	Peak position (2θ), ($^\circ$)	$2\sin\theta$	d(111)	Lattice parameter (a_{Cu})
Cu-C	43.30	0.7378	2.0873	3.615
$\text{Cu}_{90}\text{Zn}_{10}\text{-C}$	43.17	0.7358	2.0930	3.625
$\text{Cu}_{75}\text{Zn}_{25}\text{-C}$	43.03	0.7334	2.0998	3.637
$\text{Cu}_{50}\text{Zn}_{50}\text{-C}$	43.18	0.7360	2.0924	3.624

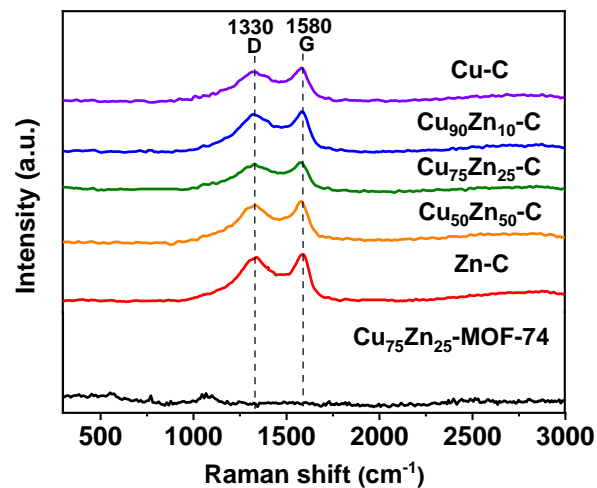


Fig. S2 Raman spectroscopy spectra of $\text{Cu}_{75}\text{Zn}_{25}\text{-MOF-74}$ and $\text{Cu}_x\text{Zn}_{100-x}\text{-C}$ using 532 nm excitation.

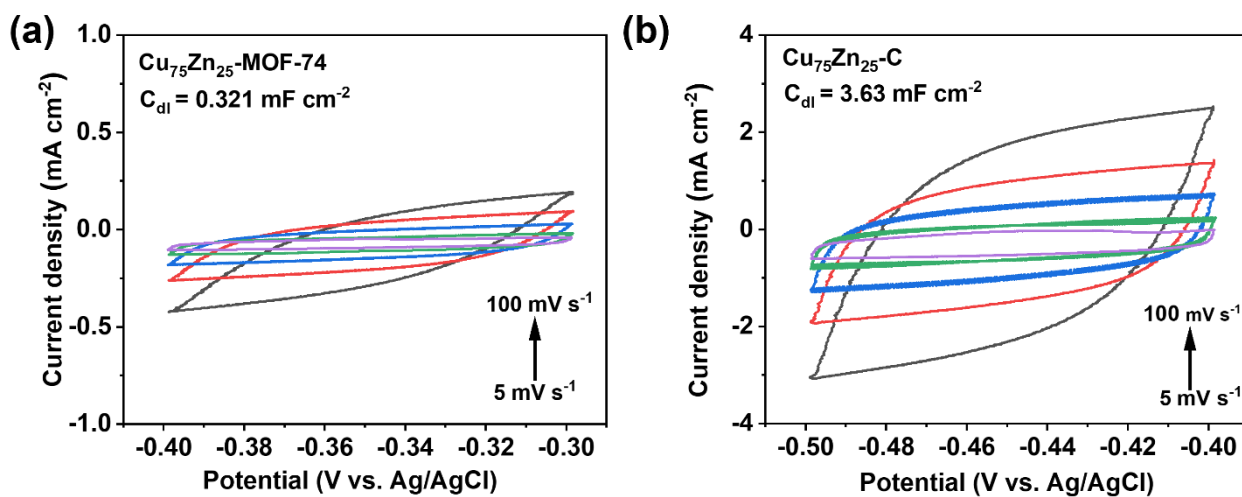


Fig. S3 CV plots as a function of scan rates of (a) $\text{Cu}_{75}\text{Zn}_{25}\text{-MOF-74}$ and (b) $\text{Cu}_{75}\text{Zn}_{25}\text{-C}$ in CO_2 -saturated 0.1 M KHCO_3 electrolytes.

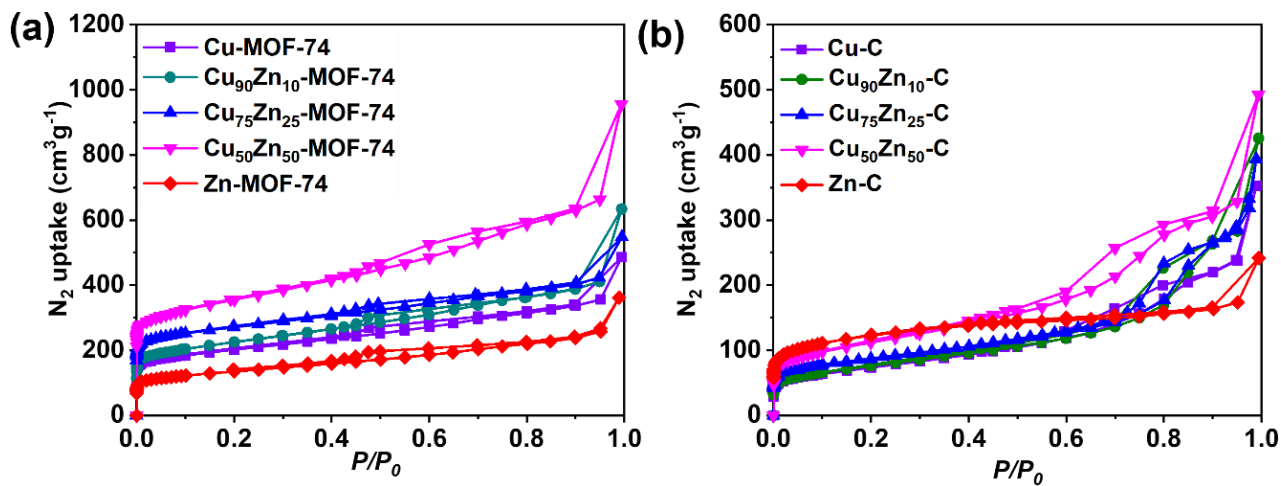


Fig. S4 N_2 adsorption-desorption isotherm of (a) $\text{Cu}_x\text{Zn}_{100-x}\text{-MOF-74}$ and (b) $\text{Cu}_x\text{Zn}_{100-x}\text{-C}$.

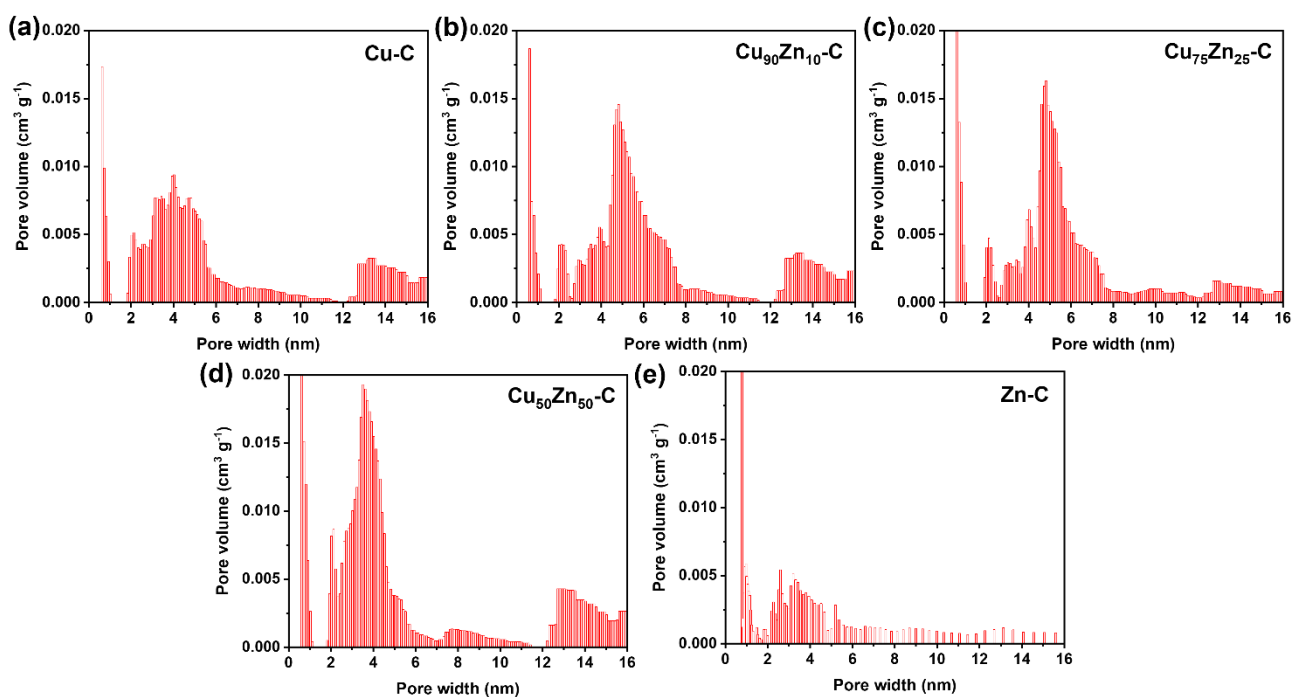


Fig. S5 Pore size distribution of (a) Cu-C, (b) Cu₉₀Zn₁₀-C, (c) Cu₇₅Zn₂₅-C, (d) Cu₅₀Zn₅₀-C, and (e) Zn-C.

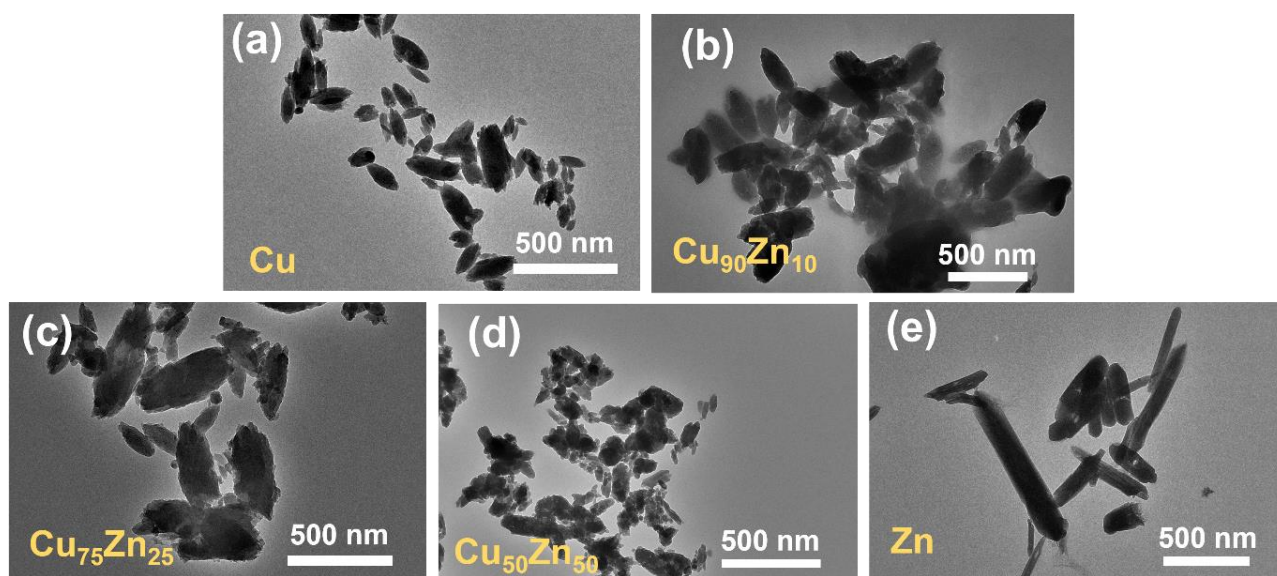


Fig. S6 TEM images of Cu_xZn_{100-x}MOF-74: (a) Cu, (b) Cu₉₀Zn₁₀, (c) Cu₇₅Zn₂₅, (d) Cu₅₀Zn₅₀, and (e) Zn.

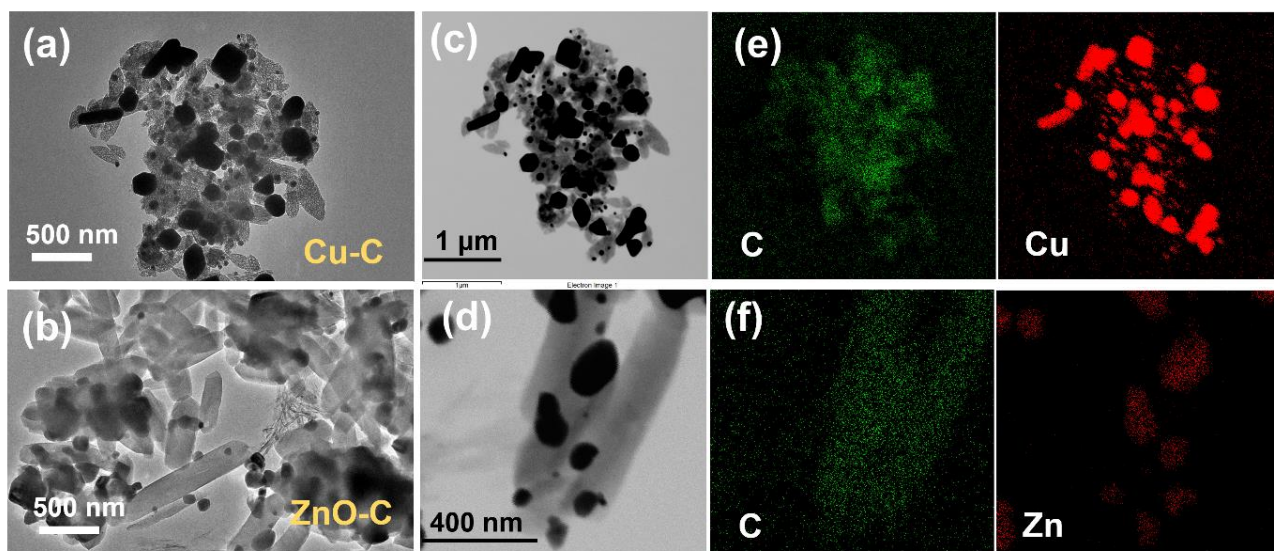


Fig. S7 TEM images and TEM-EDX mapping of (a, c, and e) Cu-C and (b, d, and f) Zn-C.

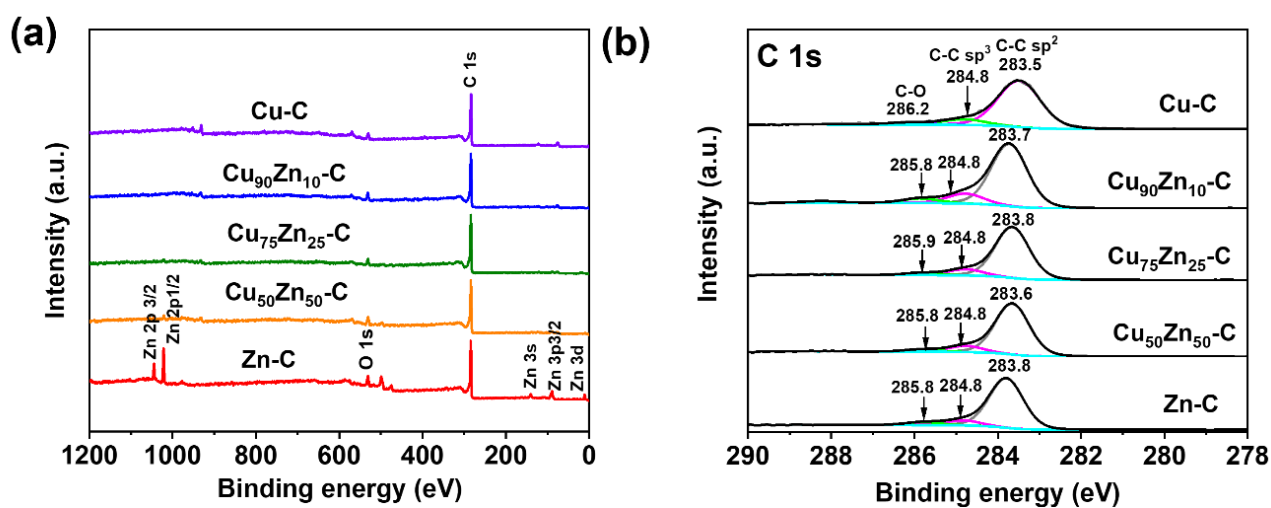


Fig. S8 (a) XPS survey spectrum and (b) C 1s spectra of $\text{Cu}_x\text{Zn}_{100-x}\text{-C}$.

Section S2: Electrochemical CO_2 reduction reaction over $\text{Cu}_x\text{Zn}_{100-x}\text{-C}$ electrocatalysts

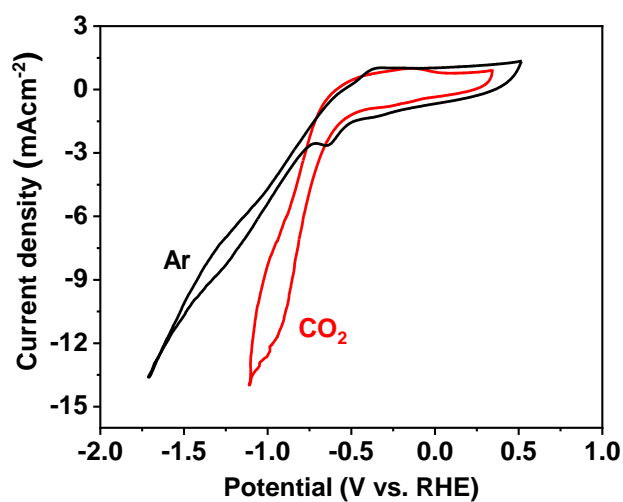


Fig. S9 Cyclic voltammogram of $\text{Cu}_{75}\text{Zn}_{25}\text{-C}$ under Ar and CO_2 atmospheres.

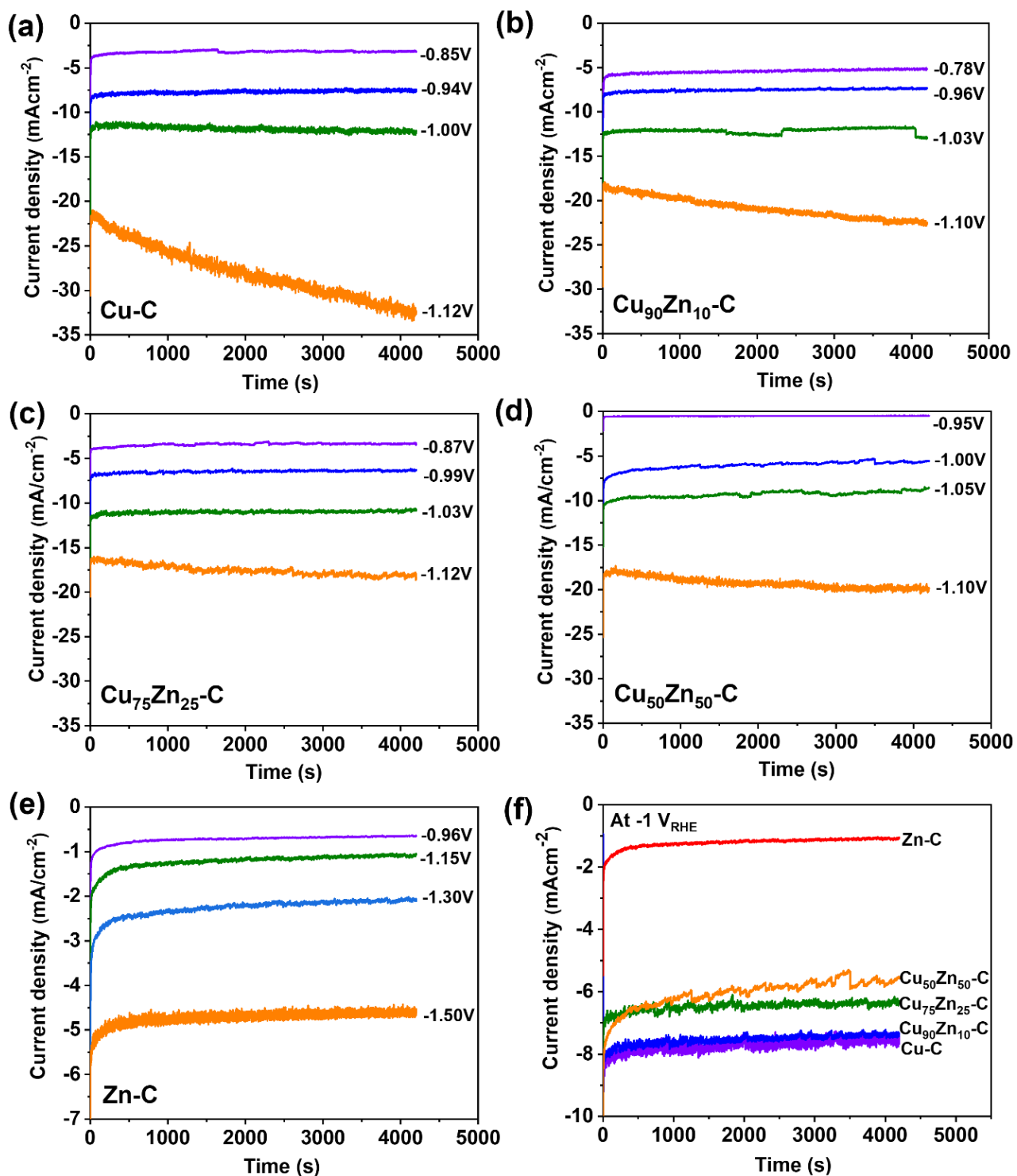


Fig. S10. Plots of current density over time with different potentials of (a) Cu-C, (b) Cu₉₀Zn₁₀-C, (c) Cu₇₅Zn₂₅-C, (d) Cu₅₀Zn₅₀-C, (e) Zn-C, and (f) Cu_xZn_{100-x}-C at -1 V vs. RHE. The increase in current density over time of Cu-C (-1.12 V) and Cu₉₀Zn₁₀-C (-1.10 V) corresponds to the increase in the HER activity (Fig. S11) which is likely due to the restructuring of Cu nanoparticles at high cathodic potentials. TEM image of the spent Cu-C shows agglomeration of Cu NPs supporting this hypothesis (Fig. S12).

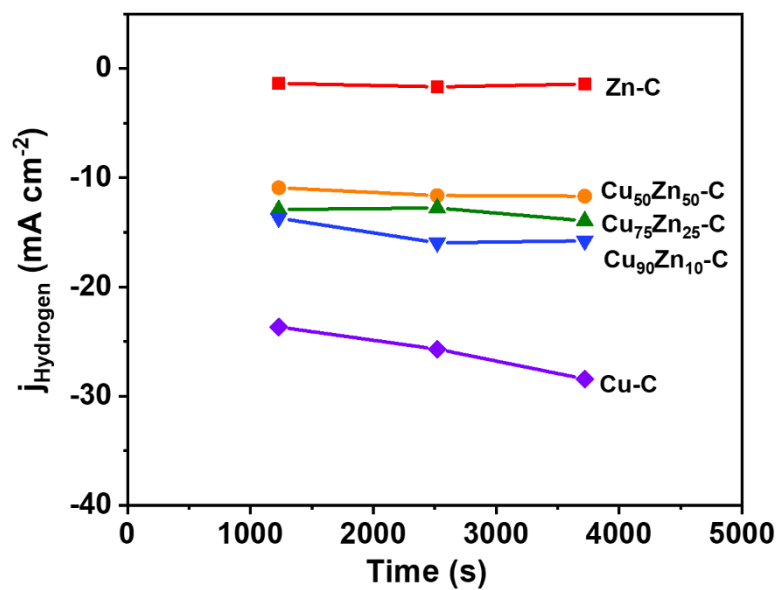


Fig. S11 HER plot between partial current density of hydrogen against reaction time at high cathodic potentials: Cu-C ($-1.12 V_{\text{RHE}}$), Cu₉₀Zn₁₀-C ($-1.10 V_{\text{RHE}}$), Cu₇₅Zn₂₅-C ($-1.12 V_{\text{RHE}}$), Cu₅₀Zn₅₀-C ($-1.10 V_{\text{RHE}}$), and Zn-C ($-1.50 V_{\text{RHE}}$).

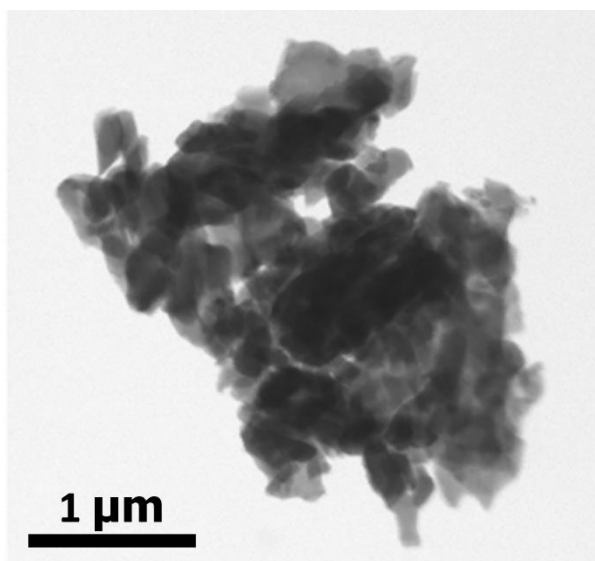


Fig. S12 TEM image of spent Cu-C after the reaction for 4200 s at $-1.12 V_{\text{RHE}}$.

Table S3 Faradaic efficiency, current density, and partial current density of C₁, C₂, and HER products using Cu-C.

Parameter	Product	Potential (V vs. RHE)			
		-0.85	-0.94	-1.00	-1.12
FE (%)	CO	7.6	4.1	0.99	0.89
	HCOOH	19	15	3.2	0.25
	C ₂ H ₄	0	3.1	3.4	0.94
	C ₂ H ₅ OH	4.7	1.7	2.2	0.85
	H ₂	18	38	60	55
Partial current density (mA cm ⁻²)	CO	0.25	0.31	0.12	0.25
	HCOOH	0.61	1.17	0.38	0.07
	C ₂ H ₄	0	0.23	0.41	0.26
	C ₂ H ₅ OH	0.15	0.13	0.26	0.24
	H ₂	0.6	2.95	7.04	27.1
Current (mA)	Total	19	46	71	117
Current density (mA cm ⁻²)	Total	3.2	8.1	12	28

Table S4 Faradaic efficiency, current density, and partial current density of C₁, C₂, and HER products using Cu₉₀Zn₁₀-C.

Parameter	Product	Potential (V vs. RHE)			
		-0.78	-0.96	-1.03	-1.10
FE (%)	CO	3.3	2.8	2.4	0.23
	HCOOH	6.9	6.3	3.0	0.17
	C ₂ H ₄	0	8.2	8.0	1.1
	C ₂ H ₅ OH	1.2	5.3	5.9	1.0
	H ₂	36.7	34.1	53.3	72.6
Partial current density (mA cm ⁻²)	CO	0.18	0.19	0.29	0.05
	HCOOH	0.38	0.41	0.36	0.04
	C ₂ H ₄	0	0.55	0.97	0.23
	C ₂ H ₅ OH	0.06	0.34	0.71	0.22
	H ₂	2.0	1.9	6.5	15.1
Current (mA)	Total	33	41	73	125
Current density (mA cm ⁻²)	Total	5.4	6.9	12	21

Table S5. Faradaic efficiency, current density, and partial current density of C₁, C₂, and HER products using Cu₇₅Zn₂₅-C.

Parameter	Product	Potential (V vs. RHE)			
		-0.87	-0.99	-1.03	-1.12
FE (%)	CO	6.7	3.0	0.88	0.28
	HCOOH	6.3	5.2	1.1	0.13
	C ₂ H ₄	9.3	15.4	10	0.82
	C ₂ H ₅ OH	1.9	7.2	6.9	1.7
	H ₂	40	37	47	75
Partial current density (mA cm ⁻²)	CO	0.23	0.20	0.10	0.05
	HCOOH	0.21	0.35	0.12	0.02
	C ₂ H ₄	0.32	1.0	1.2	0.14
	C ₂ H ₅ OH	0.06	0.47	0.75	0.30
	H ₂	1.4	2.5	5.2	13.2
Current (mA)	Total	21	39	66	105
Current density (mA cm ⁻²)	Total	3.4	6.7	11	18

Table S6 Faradaic efficiency, current density, and partial current density of C₁, C₂, and HER products using Cu₅₀Zn₅₀-C.

Parameter	Product	Potential (V vs. RHE)			
		-0.95	-0.99	-1.05	-1.10
FE (%)	CO	22	10	4.7	0.97
	HCOOH	1.7	2.9	1.2	0.24
	C ₂ H ₄	0	5.8	11	7.6
	C ₂ H ₅ OH	0	5.4	11.4	6.3
	H ₂	0	28	32	59
Partial current density (mA cm ⁻²)	CO	0.11	0.59	0.40	0.19
	HCOOH	0.01	0.16	0.11	0.05
	C ₂ H ₄	0	0.34	0.99	1.4
	C ₂ H ₅ OH	0	0.32	1.1	1.2
	H ₂	0	0.96	0.41	0.31
Current (mA)	Total	3.1	35	56	116
Current density (mA cm ⁻²)	Total	0.51	5.8	9.3	19

Table S7 Faradaic efficiency, current density, and partial current density of C₁, C₂, and HER products using Zn-C.

Parameter	Product	Potential (V vs. RHE)			
		-0.96	-1.15	-1.30	-1.50
FE (%)	CO	19	36	44	34
	HCOOH	1.8	1.9	1.8	3.6
	C ₂ H ₄	0	0	0	0
	C ₂ H ₅ OH	0	0	0	0
	H ₂	0	0	0	31
Partial current density (mA cm ⁻²)	CO	0.13	0.37	1.0	1.6
	HCOOH	0.01	0.02	0.04	0.17
	C ₂ H ₄	0	0	0	0
	C ₂ H ₅ OH	0	0	0	0
	H ₂	0	0	0	1.5
Current (mA)	Total	4.3	6.1	13.6	28.3
Current density (mA cm ⁻²)	Total	0.7	1.0	2.3	4.7

Table S8 Comparison of performance of CuZn electrocatalysts reported in the literature for the CO₂RR to C₂ products.

Catalyst	Condition	FE (%)		FE _{C₂} enhancement CuZn/Cu (times)	Total current density (mA cm ⁻²)	Ref
		Ethylene	C ₂			
Cu ₉ Zn ₁	0.1 M KHCO ₃ -1.1 V _{RHE} , H-cell	17	25	1.7	-	1
Cu ₄ Zn ₁	0.1 M KHCO ₃ -1.1 V _{RHE} , H-cell	33.3	33.3	2.2	6.1	2
Cu/ZnO(101̄0)	0.1 M KHCO ₃ -1.4 V _{Ag/AgCl} , H-cell	10.1	20.3	1.8	12	3
CuZn-1	0.1 M KHCO ₃ -1.1 V _{RHE} , H-cell	14	14	-	6	4
Cu ₄ Zn ₁	0.1 M KHCO ₃ -1.05 V _{RHE} , H-cell	10	40	2.4	-	5
HMMP Cu ₅ Zn ₈	0.1 M KHCO ₃ -0.8 V _{RHE} , H-cell	-	58	7.2	4.3	6
CuZn ₂₀ /NGN	0.1 M KHCO ₃ -0.8 V _{RHE} , H-cell	-	34.2 5	6.8	3.95	7
Cu/ZnO	1 M KOH -0.8 V _{RHE} , Flow cell	49	78	1.2	600	8
CuO/ZnO/C	1 M KOH -0.75 V _{RHE} , Flow cell	50.9	74	1.5	367	9
Cu ₇₅ Zn ₂₅ -C	0.1 M KHCO ₃ -1 V _{RHE} , H-cell	15	23	4.7	6.7	This work

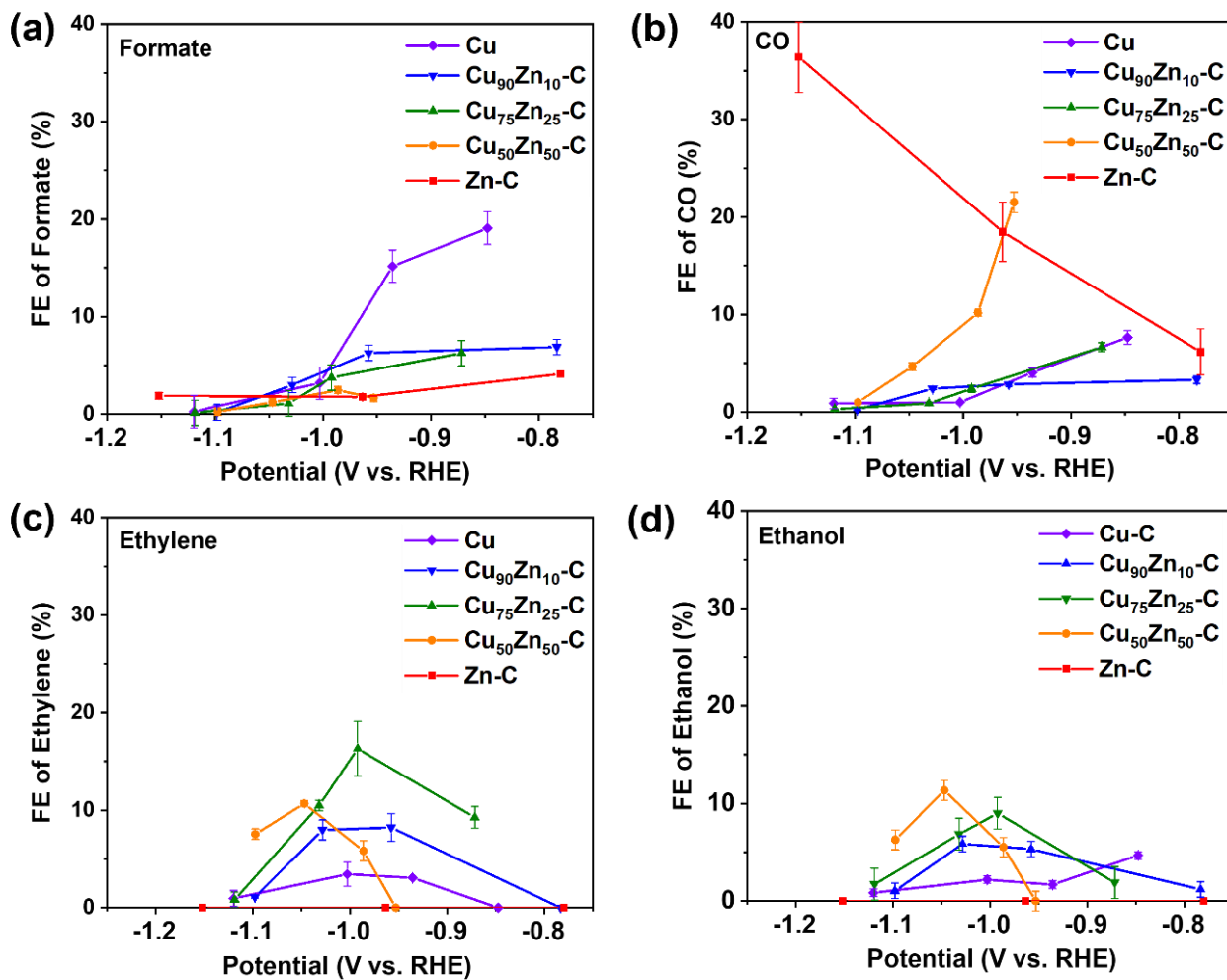


Fig. S13 Faradaic efficiency of detected products using $\text{Cu}_x\text{Zn}_{100-x}\text{-C}$: (a) formate, (b) CO, (c) ethylene, and (d) ethanol.

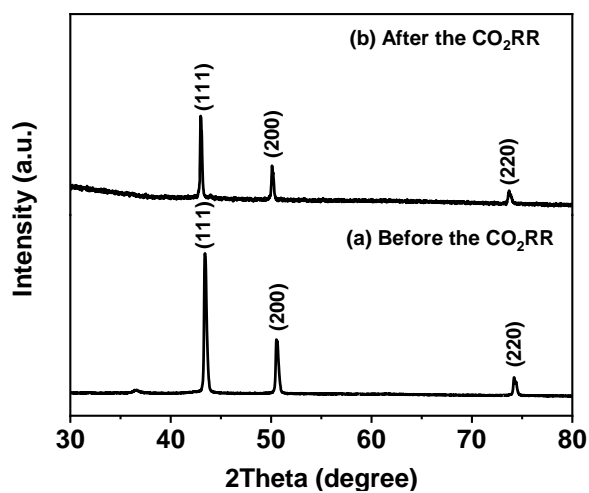


Fig. S14 XRD results of $\text{Cu}_{75}\text{Zn}_{25}\text{-C}$ (a) before and (b) after the CO_2RR .

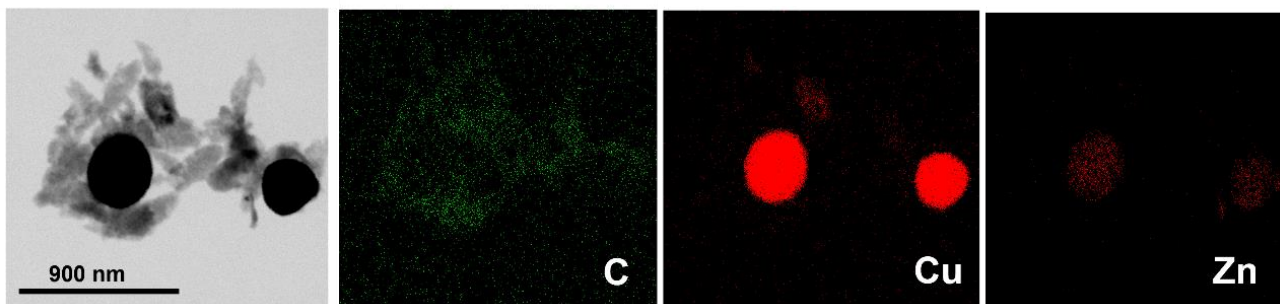


Fig. S15 EDS image and mapping (C, Cu, and Zn) of $\text{Cu}_{75}\text{Zn}_{75}\text{-C}$ after the CO_2RR .

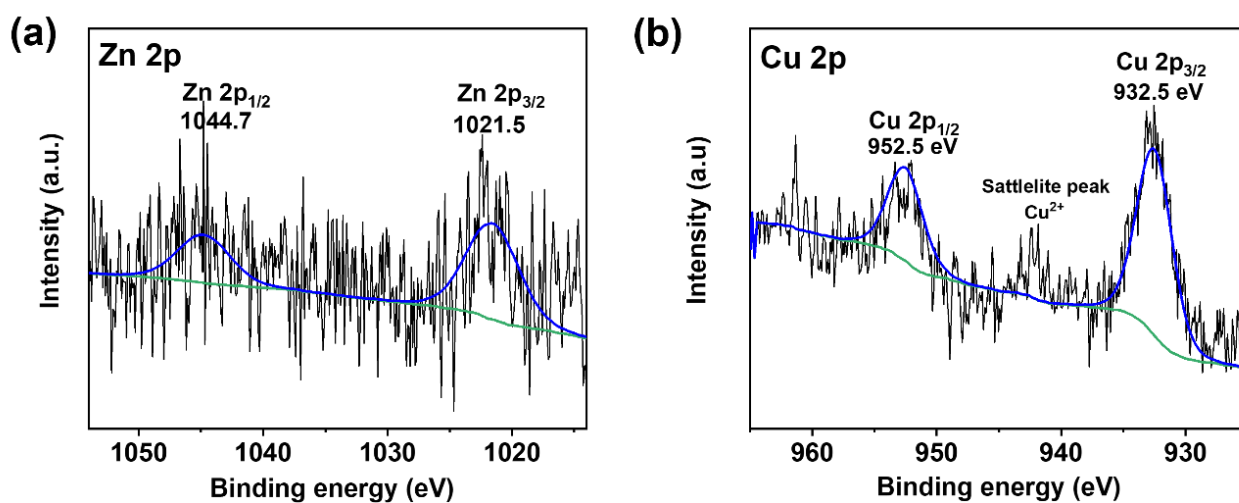


Fig. S16 XPS High-resolution spectra of (a) Zn 2p orbital and (b) Cu 2p of $\text{Cu}_{75}\text{Zn}_{25}\text{-C}$ after the CO_2RR .

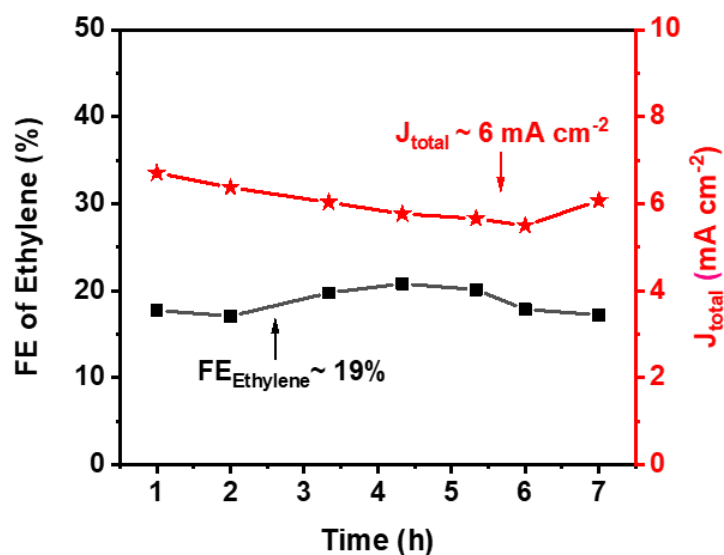


Fig. S17 Stability test of $\text{Cu}_{75}\text{Zn}_{25}\text{-C}$ in 0.1 M KHCO_3 .

Section S3. DFT calculations

S3.1 Computational details

The Cu₃Zn(111) alloy and Cu(111) were chosen as the representative for the experimental suggestion of Cu₇₅Zn₂₅ alloy catalyst and pure Cu catalyst, respectively. The surface models were constructed using a supercell size of 2 × 2 with four atomic layers in which the two bottom layers were fixed during optimization. The number of atomic layers in a slab model were checked with the convergence of *CO adsorption energy. The vacuum space of 35 Å in the z-direction was added to avoid the interactions between the periodic images. The Monkhorst-Pack mesh sampling¹⁰ k-points of 4 × 4 × 1 was applied. The convergence test of the number of k-points (2 × 2 × 1, 3 × 3 × 1, 4 × 4 × 1 and 5 × 5 × 1) were performed. The difference between the adsorption energies at a k-points of 4 × 4 × 1 and 5 × 5 × 1 was 0.03 eV for Cu₃Zn surface, thus k-points of 4 × 4 × 1 was used in this work.

To prepare the initial surface models with explicit solvent, we carried out ab initio molecular dynamics (AIMD) simulation of ten water layers on Cu₃Zn(111) surfaces at 300 K for 3 ps, including a total of 90 water molecules. The AIMD snapshots for the equilibrium ten water layers on Cu₃Zn(111) is presented in Fig. S18a

According to the theoretical studies of solvent–adsorbate interactions on Cu(211) surface using AIMD¹¹ simulations and the study of solvent effects on CO₂ reduction pathways on Cu(100) surface using DFT calculations,¹² the first water layer was found to be the most important layer as interactions between water molecules and adsorbates could significantly affect adsorbate stability and the reaction pathways. The second water layer was found to interact with the first water layer and has less interaction with the adsorbates. Therefore, to mimic the solvent environment and keep affordable computational cost, two water layers near the interface were included in a surface model for all DFT calculations. All atoms including an adsorbed intermediate molecule, water molecules and the top two surface layers were allowed to relax during DFT calculations. The Cu₃Zn(111) alloy and Cu(111) surface models which were used in this study are shown in Fig. S18b. The surface models contain a total of 64 metal atoms and 20 water molecules.

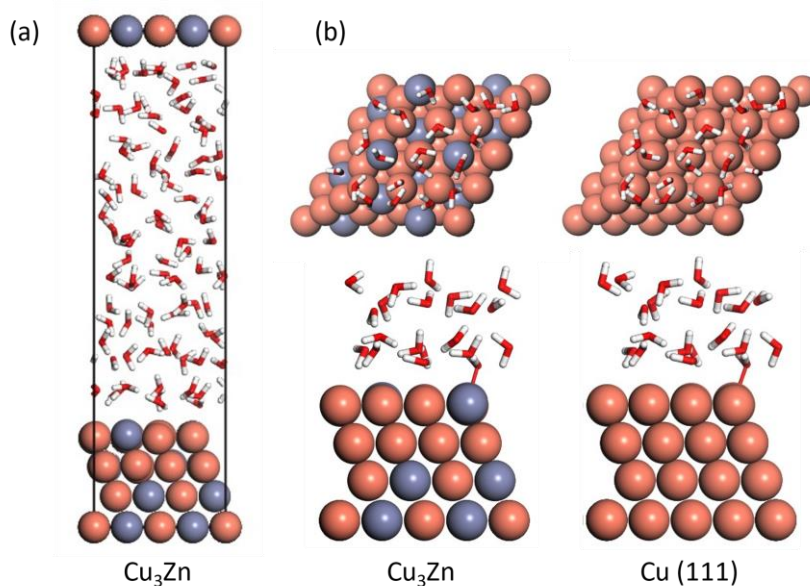


Fig. S18. The explicit water models on Cu₃Zn(111) and Cu(111) surfaces. (a) side view of ten water layers on Cu₃Zn(111) surface model obtained from AIMD simulation of 3 ps. (b) top and side views of Cu₃Zn(111) and Cu(111) surface models with two water layers.

S3.2 Free energy calculations and pathway free energy diagrams

Free energy (G) is obtained from the thermodynamic calculations as a function of the enthalpy (H) and entropy (S) shown in equation (S1) and (S2). The thermodynamic terms are derived from the vibrational frequency calculations.

$$G = H - TS \quad (\text{S1})$$

$$G = E_{\text{Electronic}} + \text{ZPE} + \int C_p dT - TS \quad (\text{S2})$$

where $E_{\text{Electronic}}$, ZPE , $\int C_p dT$ and TS are electronic energy from DFT calculations, zero-point energy, enthalpic and entropic correction term calculated at 300 K, respectively.

The vibrational frequency and free energies of all intermediates and adsorbed configurations were computed. Furthermore, the vibrational frequency calculations were also performed to confirm the transition states in the *CO–*CO coupling reaction in which one imaginary frequency was found. The vibrational frequencies that lower than the value of 50 cm⁻¹ were replaced by the value of 50 cm⁻¹ before computing enthalpic and entropic correction terms in order to exclude the cause of a breakdown in the harmonic oscillator approximation¹³.

The correction term for the gas-phase is needed for free energy calculations of the gas-phase molecules. We applied the RPBE gas-phase free energies corrections as suggested by Peterson et al.¹⁴ The water molecules require further correction in terms of liquid-phase water molecules (H₂O (l)).^{15,16} The corrections terms and free

energies of H_2 (g), H_2O (g), CO (g) and H_2O (l) were reported in our previous theoretical study for CO_2RR in the explicit water models.¹²

To construct a pathway diagram, the relative free energy at each elementary step was calculated. The free energy change of each step that involves an electrochemical proton-electron transfer will be a function of the applied electrode potential. The computational hydrogen electrode (CHE) model proposed by Nørskov et al.¹⁶ was applied to account the effect of electrode potential. In this technique, zero voltage is defined based on the reversible hydrogen electrode (RHE). In this study, the pathway diagrams were constructed at $-1 \text{ V}_{\text{RHE}}$. Peterson et al.⁵ described details of computational hydrogen electrode technique.

All considered pathways in this study are shown in Fig. S19 including proton-electron transfer and C–O bond breaking steps. As discussed in the main text, the pathways beyond $^*\text{CHCO}$ (3a) intermediate which is the product of the third proton-electron transfer step shown in the previous study³ were explored in this work. The free energy diagrams of all possible pathways toward ethylene and ethanol on $\text{Cu}_3\text{Zn}(111)$ and $\text{Cu}(111)$ surfaces are presented in Fig. S20 and Fig. S21, respectively.

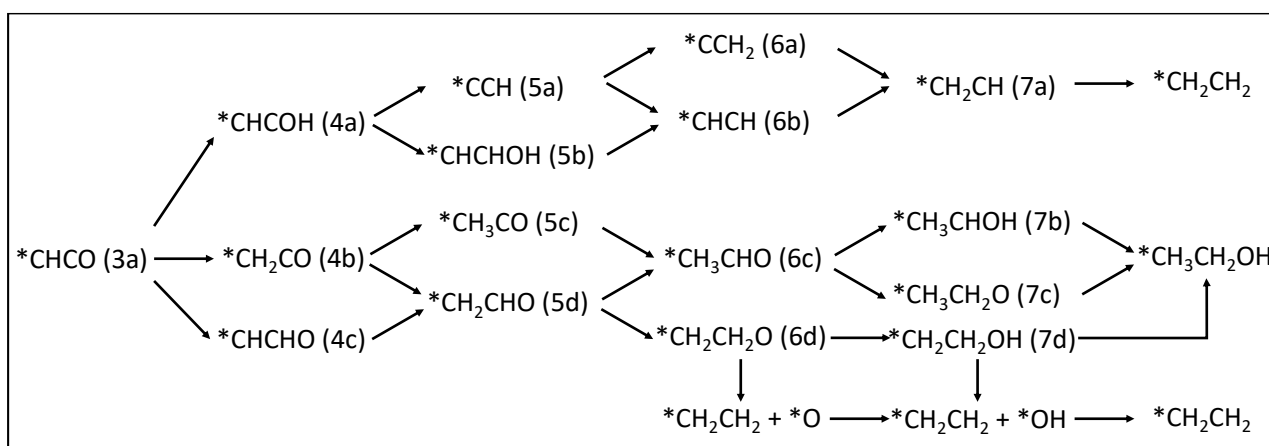
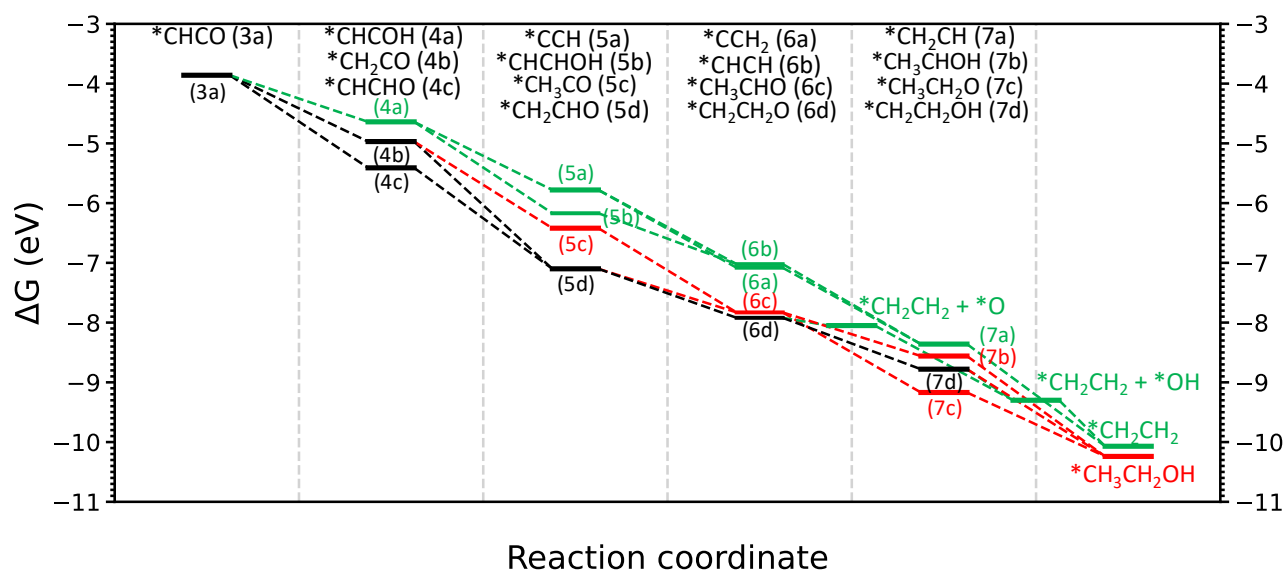
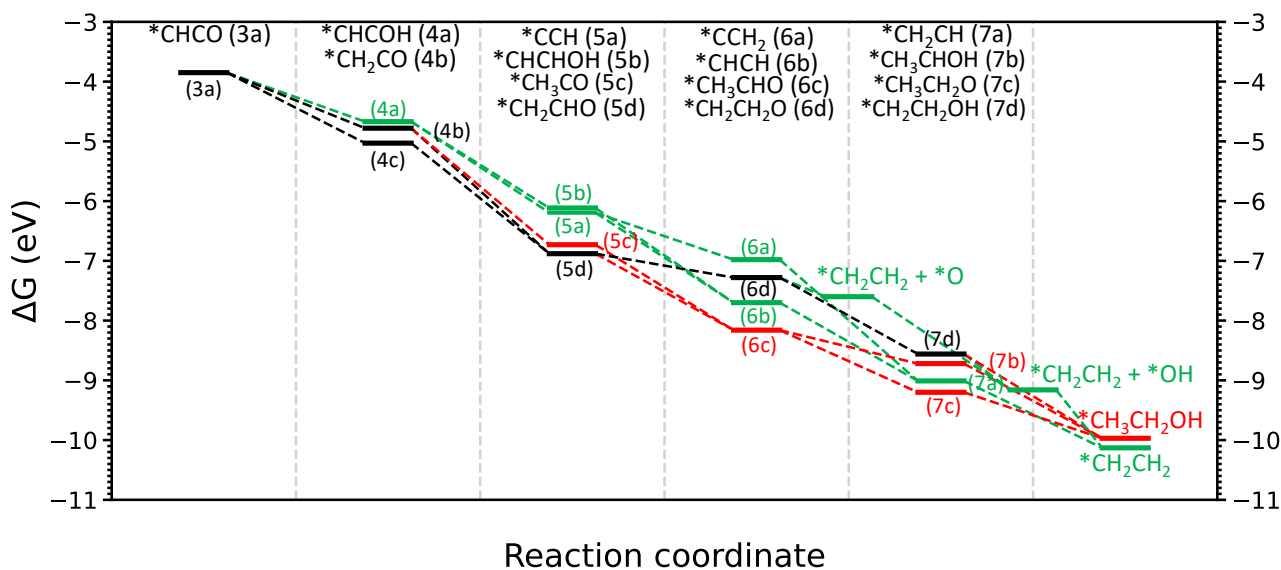


Fig. S19 All considered CO_2RR pathways toward ethylene and ethanol starting from $^*\text{CHCO}$ (3a) intermediate.



Reactions	ΔG (eV)	Reactions	ΔG (eV)
$4 H^+/e^-$ (3a) \rightarrow (4a)	-0.78	$5 H^+/e^-$ (4a) \rightarrow (5a)	-1.14
(3a) \rightarrow (4b)	-1.11	(4a) \rightarrow (5b)	-1.53
(3a) \rightarrow (4c)	-1.55	(4b) \rightarrow (5c)	-1.45
		(4b) \rightarrow (5d)	-2.13
		(4c) \rightarrow (5d)	-1.68
$6 H^+/e^-$ (5a) \rightarrow (6a)	-1.28	$7 H^+/e^-$ (6a) \rightarrow (7a)	-1.30
(5a) \rightarrow (6b)	-1.26	(6b) \rightarrow (7a)	-1.32
(5b) \rightarrow (6b)	-0.87	(6c) \rightarrow (7b)	-0.71
(5c) \rightarrow (6c)	-1.43	(6c) \rightarrow (7c)	-1.32
(5d) \rightarrow (6c)	-0.75	(6d) \rightarrow (7d)	-0.88
(5d) \rightarrow (6d)	-0.81		
$8 H^+/e^-$ (7a) \rightarrow *CH ₂ CH ₂	-1.71	<i>After the 6 H⁺/e⁻ step</i> (6d) \rightarrow *CH ₂ CH ₂ + *O	-0.14
(7b) \rightarrow *CH ₃ CH ₂ OH	-1.68	*CH ₂ CH ₂ + *O \rightarrow	-1.25
(7c) \rightarrow *CH ₃ CH ₂ OH	-1.07	*CH ₂ CH ₂ + *OH	
(7d) \rightarrow *CH ₃ CH ₂ OH	-1.45	<i>After the 7 H⁺/e⁻ step</i> (7d) \rightarrow *CH ₂ CH ₂ + *OH	-0.52
		*CH ₂ CH ₂ + *OH \rightarrow	-0.77
		*CH ₂ CH ₂	

Fig. S20 Relative free energy diagrams of all possible pathways to ethylene and ethanol on Cu₃Zn(111) surface at $U = -1 V_{RHE}$. The relative energies are referenced to two *CO adsorbed on the surface. Green, red, and black arrows show reaction steps leading to (i) only ethylene, (ii) only ethanol and (iii) both ethylene and ethanol, respectively.



Reactions	ΔG (eV)	Reactions	ΔG (eV)
$4 H^+/e^-$ (3a) \rightarrow (4a)	-0.82	$5 H^+/e^-$ (4a) \rightarrow (5a)	-1.51
(3a) \rightarrow (4b)	-0.93	(4a) \rightarrow (5b)	-1.46
(3a) \rightarrow (4c)	-1.18	(4b) \rightarrow (5c)	-1.95
		(4b) \rightarrow (5d)	-2.10
		(4c) \rightarrow (5d)	-1.85
$6 H^+/e^-$ (5a) \rightarrow (6a)	-0.80	$7 H^+/e^-$ (6a) \rightarrow (7a)	-2.02
(5a) \rightarrow (6b)	-1.52	(6b) \rightarrow (7a)	-1.31
(5b) \rightarrow (6b)	-1.57	(6c) \rightarrow (7b)	-0.56
(5c) \rightarrow (6c)	-1.43	(6c) \rightarrow (7c)	-1.05
(5d) \rightarrow (6c)	-1.28	(6d) \rightarrow (7d)	-1.28
(5d) \rightarrow (6d)	-0.41		
$8 H^+/e^-$ (7a) \rightarrow *CH_2CH_2	-1.12	<i>After the 6 H^+/e^- step</i> (6d) \rightarrow $^*CH_2CH_2 + ^*O$	-0.32
(7b) \rightarrow *CH_3CH_2OH	-1.25	$^*CH_2CH_2 + ^*O \rightarrow$ $^*CH_2CH_2 + ^*OH$	-1.88
(7c) \rightarrow *CH_3CH_2OH	-0.76	(7d) \rightarrow $^*CH_2CH_2 + ^*OH$	-0.60
(7d) \rightarrow *CH_3CH_2OH	-1.41	<i>After the 7 H^+/e^- step</i> $^*CH_2CH_2 + ^*OH \rightarrow$ *CH_2CH_2	-0.97

Fig. S21 Relative free energy diagrams of all possible pathways to ethylene and ethanol on Cu(111) surface at $U = -1 V_{RHE}$. The relative energies are referenced to two *CO adsorbed on the surface. Green, red, and black arrows show reaction steps leading to (i) only ethylene, (ii) only ethanol and (iii) both ethylene and ethanol, respectively.

S3.3 Intermediate adsorption

Various adsorbed intermediate configurations at every possible binding site were explored on $\text{Cu}_3\text{Zn}(111)$ and $\text{Cu}(111)$ surfaces. Fig. S22 illustrates the binding sites on $\text{Cu}_3\text{Zn}(111)$ (Fig. S22a) and $\text{Cu}(111)$ (Fig. S18b) surfaces. Four distinguishable binding sites are presented on $\text{Cu}(111)$ surface (Fig. S22b). There are nine possible distinct sites on $\text{Cu}_3\text{Zn}(111)$ surface (Fig. S21a) i.e., two of the on-top sites which are the on-top Cu (site 1) and the on-top Zn (site 2) sites, three of the bridge sites of the Cu–Cu bridge with Cu subatomic (site 3), the Cu–Cu bridge with Zn subatomic (site 4) and the Cu–Zn bridge (site 5), two of the hcp hollow sites including the hcp(Cu–Cu–Cu) hollow with Zn subatomic (site 6) and the hcp(Cu–Cu–Zn) hollow with Cu subatomic (site 7) and two of the fcc hollow sites including the fcc(Cu–Cu–Cu) (site 8) and the fcc (Cu–Cu–Zn) (site 9).

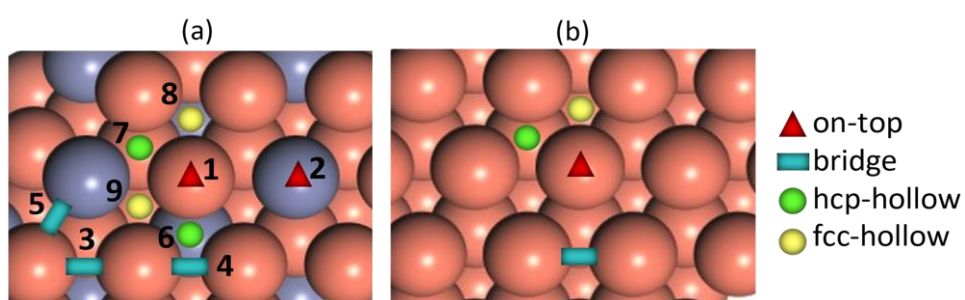


Fig. S22 Binding sites on (a) $\text{Cu}_3\text{Zn}(111)$ and (b) $\text{Cu}(111)$ surfaces.

Table S9. The optimized adsorption configurations and adsorption free energy (G_{ads}) of the intermediates on $\text{Cu}_3\text{Zn}(111)$ and $\text{Cu}(111)$ surfaces. The solvent water molecules are not shown in snapshots.

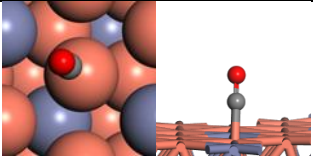
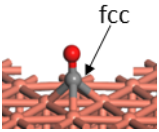
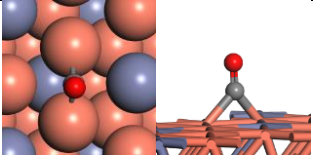
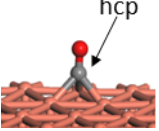
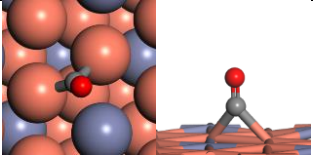
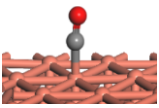
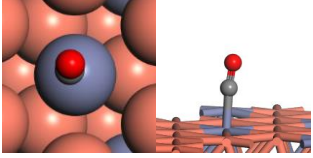
Label	Formula	Cu_3Zn		$\text{Cu}(111)$	
		Configuration	G_{ads} (eV)	Configuration	G_{ads} (eV)
–	*CO		–0.45	 fcc	–0.39
			–0.37	 hcp	–0.35
			0.00		0.08
			0.84	–	–

Table S9. The optimized adsorption configurations and adsorption free energy (G_{ads}) of the intermediates on $\text{Cu}_3\text{Zn}(111)$ and $\text{Cu}(111)$ surfaces. The solvent water molecules are not shown in snapshots. (cont.)

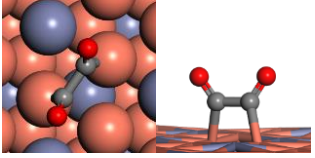
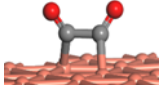
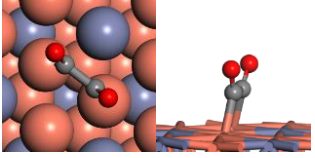
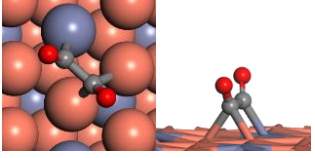
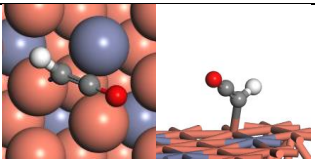
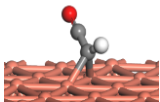
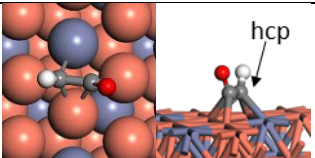
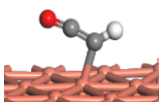
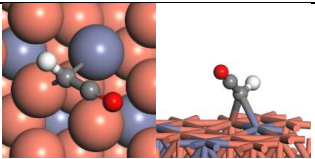
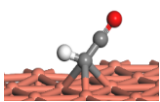
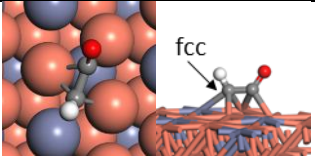
Label	Formula	Cu_3Zn		$\text{Cu}(111)$	
		Configuration	G_{ads} (eV)	Configuration	G_{ads} (eV)
–	*OCCO		–2.84		–2.42
			–2.61	–	–
			–2.19	–	–
$3 H^+/e^-$					
3a	*CHCO		–2.98		–2.91
			–2.95		–2.69
			–2.69		–2.63
			–2.67	–	–

Table S9. The optimized adsorption configurations and adsorption free energy (G_{ads}) of the intermediates on $\text{Cu}_3\text{Zn}(111)$ and $\text{Cu}(111)$ surfaces. The solvent water molecules are not shown in snapshots. (cont.)

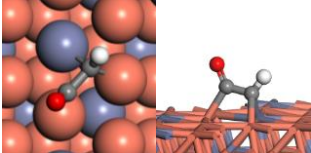
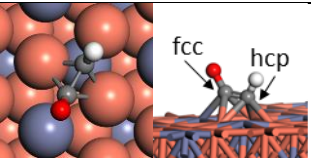
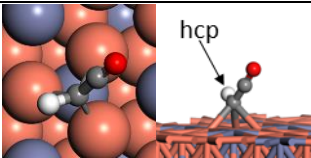
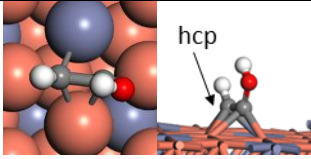
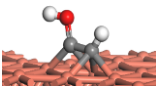
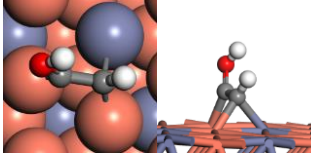
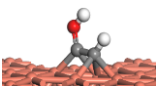
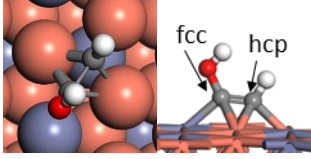
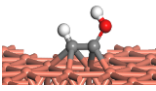
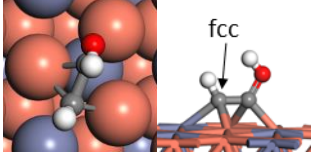
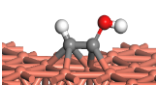
Label	Formula	Cu_3Zn		$\text{Cu}(111)$	
		Configuration	G_{ads} (eV)	Configuration	G_{ads} (eV)
$3 H^+/e^-$					
3a (cont.)	*CHCO		-2.59	—	—
			-2.57	—	—
			-2.54	—	—
$4 H^+/e^-$					
4a	*CHCOH		-1.92		-1.90
			-1.62		-1.83
			-1.57		-1.63
			-1.54		-1.62

Table S9. The optimized adsorption configurations and adsorption free energy (G_{ads}) of the intermediates on $\text{Cu}_3\text{Zn}(111)$ and $\text{Cu}(111)$ surfaces. The solvent water molecules are not shown in snapshots. (cont.)

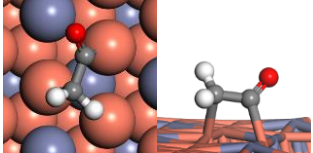
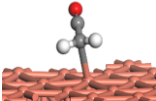
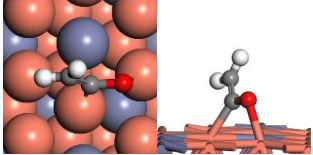
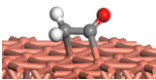
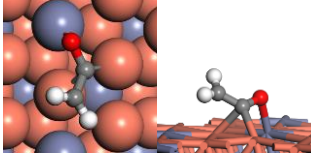
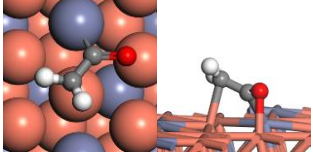
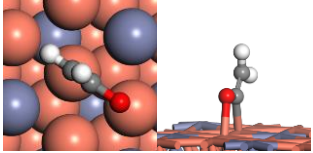
Label	Formula	Cu_3Zn		$\text{Cu}(111)$	
		Configuration	G_{ads} (eV)	Configuration	G_{ads} (eV)
$4 H^+/e^-$					
4b	* CH_2CO		-0.60		-0.35
			-0.52		-0.13
			-0.44	—	—
			-0.42	—	—
			-0.31	—	—

Table S9. The optimized adsorption configurations and adsorption free energy (G_{ads}) of the intermediates on $\text{Cu}_3\text{Zn}(111)$ and $\text{Cu}(111)$ surfaces. The solvent water molecules are not shown in snapshots. (cont.)

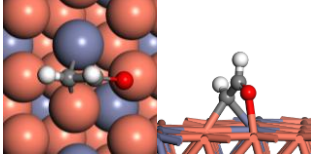
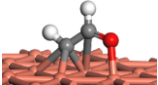
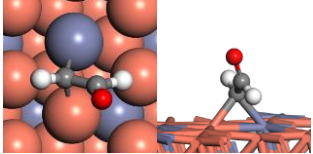

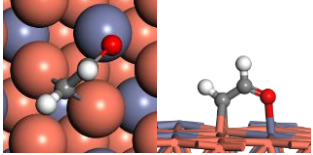

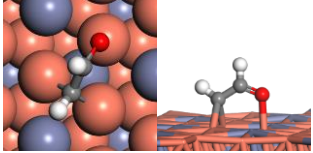
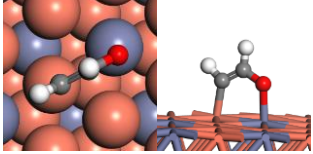
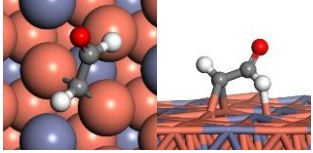
Label	Formula	Cu_3Zn		$\text{Cu}(111)$	
		Configuration	G_{ads} (eV)	Configuration	G_{ads} (eV)
$4 H^+/e^-$					
4c	*CHCHO		-4.17		-3.74
			-3.96		-3.58
			-3.89		-3.41
			-3.76	—	—
			-3.72	—	—
			-3.67	—	—

Table S9. The optimized adsorption configurations and adsorption free energy (G_{ads}) of the intermediates on $\text{Cu}_3\text{Zn}(111)$ and $\text{Cu}(111)$ surfaces. The solvent water molecules are not shown in snapshots. (cont.)

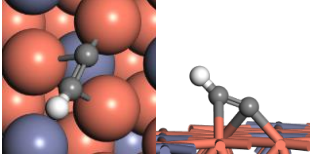
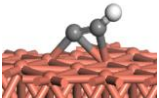
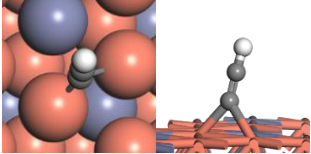
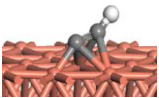
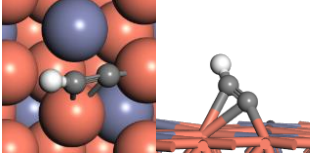
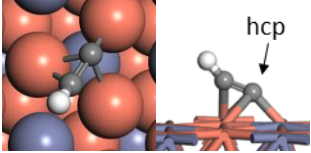
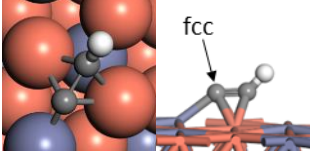
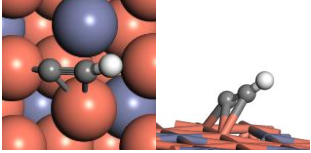
Label	Formula	Cu_3Zn		$\text{Cu}(111)$	
		Configuration	G_{ads} (eV)	Configuration	G_{ads} (eV)
$5 H^+/e^-$					
5a	*CCH		-4.72		-5.07
			-4.67		-4.50
			-4.59	—	—
			-4.49	—	—
			-4.33	—	—
			-4.21	—	—

Table S9. The optimized adsorption configurations and adsorption free energy (G_{ads}) of the intermediates on $\text{Cu}_3\text{Zn}(111)$ and $\text{Cu}(111)$ surfaces. The solvent water molecules are not shown in snapshots. (cont.)

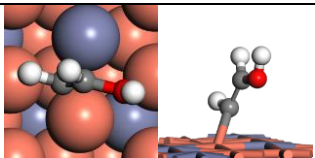

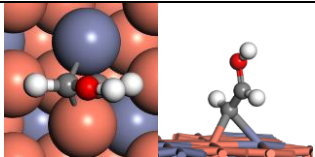
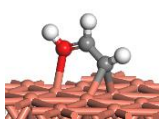
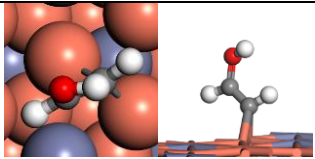
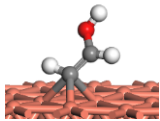
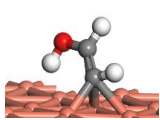
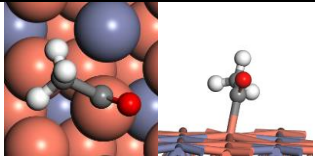
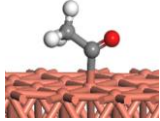
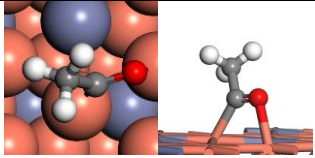
Label	Formula	Cu_3Zn		$\text{Cu}(111)$	
		Configuration	G_{ads} (eV)	Configuration	G_{ads} (eV)
$5 H^+/e^-$					
5b	*CHCHOH		-3.45		-3.35
			-3.35		-3.34
			-2.98		-3.25
		—	—		-3.10
5c	*CH ₃ CO		-1.89		-2.15
			-1.83	—	—

Table S9. The optimized adsorption configurations and adsorption free energy (G_{ads}) of the intermediates on $\text{Cu}_3\text{Zn}(111)$ and $\text{Cu}(111)$ surfaces. The solvent water molecules are not shown in snapshots. (cont.)

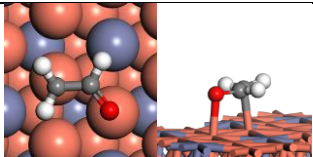
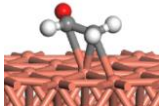
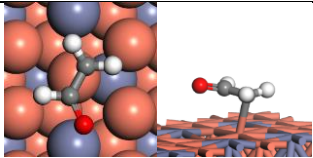
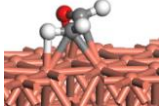
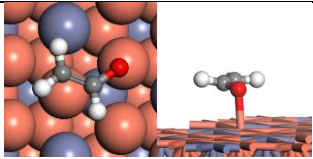
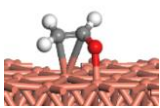
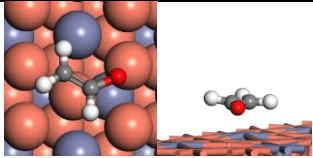
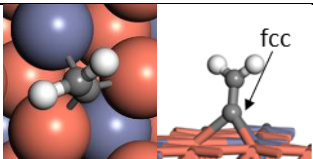
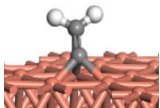
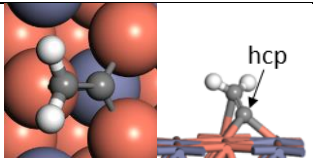
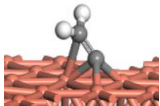
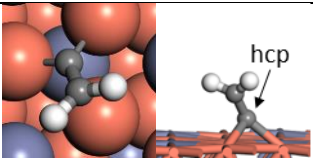
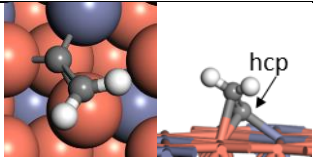
Label	Formula	Cu_3Zn		$\text{Cu}(111)$	
		Configuration	G_{ads} (eV)	Configuration	G_{ads} (eV)
$5 H^+/e^-$					
5d	* CH_2CHO		-2.89		-2.62
			-2.58		-2.08
			-2.41		-2.06
			-2.38	—	—
$6 H^+/e^-$					
6a	* CCH_2		-2.84		-2.71
			-2.70		-2.37
			-2.65	—	—
			-2.34	—	—

Table S9. The optimized adsorption configurations and adsorption free energy (G_{ads}) of the intermediates on $\text{Cu}_3\text{Zn}(111)$ and $\text{Cu}(111)$ surfaces. The solvent water molecules are not shown in snapshots. (cont.)

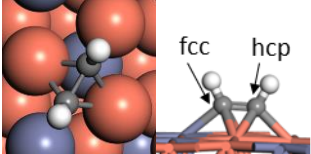

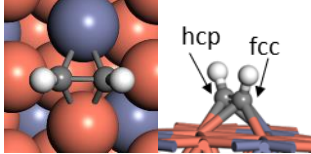
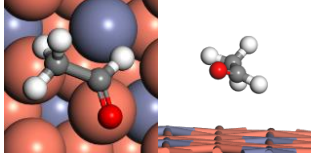
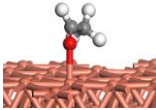
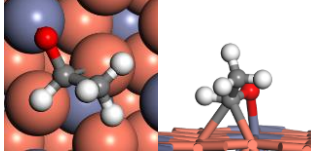
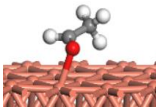
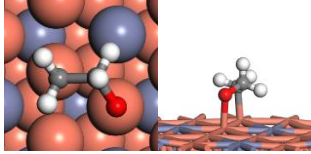

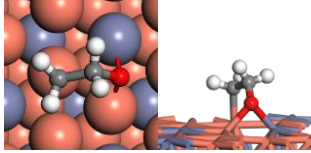
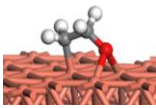
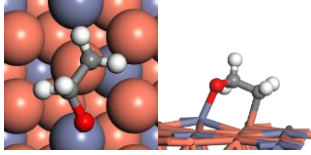
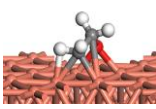
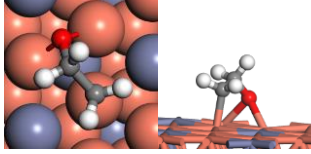
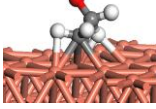
Label	Formula	Cu_3Zn		$\text{Cu}(111)$	
		Configuration	G_{ads} (eV)	Configuration	G_{ads} (eV)
$6H^+/e^-$					
6b	*CHCH	 fcc	-1.05		-1.66
		 hcp	-0.82	—	—
6c	*CH ₃ CHO		-0.57		-0.83
			-0.25		0.30
6d	*CH ₂ CH ₂ O		-0.61		0.06
			-0.35		0.28
			-0.11		0.37
			-0.03		0.64

Table S9. The optimized adsorption configurations and adsorption free energy (G_{ads}) of the intermediates on $\text{Cu}_3\text{Zn}(111)$ and $\text{Cu}(111)$ surfaces. The solvent water molecules are not shown in snapshots. (cont.)

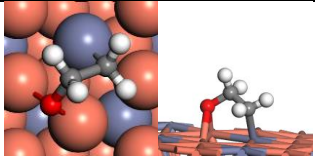
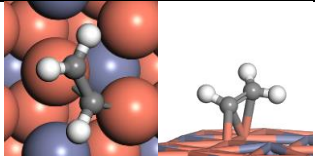

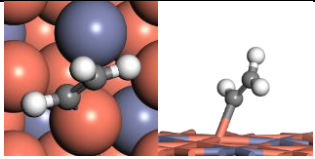
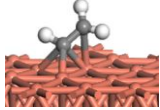
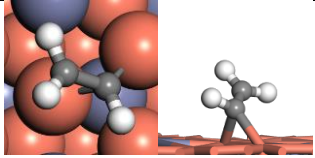
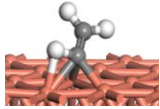
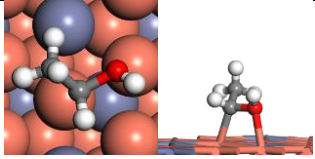
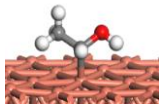
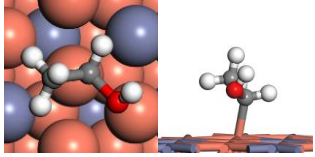
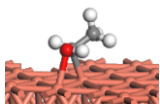
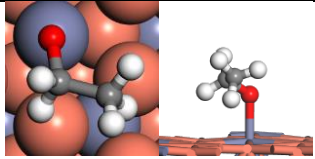
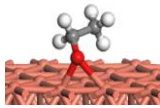
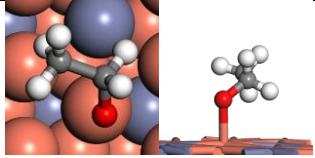
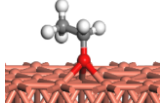
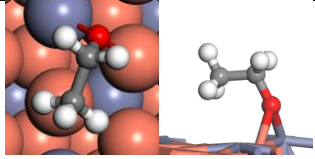
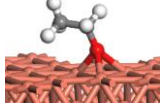
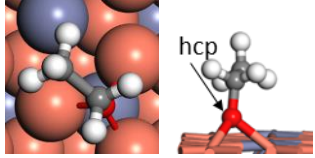
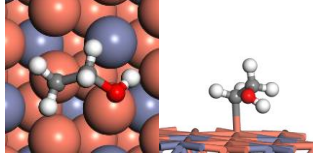
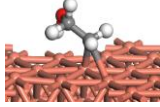
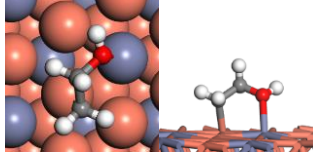
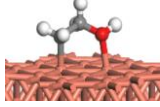
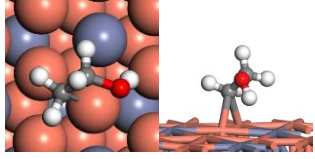
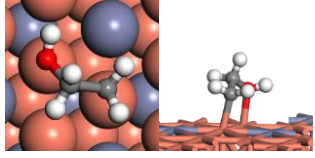
Label	Formula	Cu_3Zn		$\text{Cu}(111)$	
		Configuration	G_{ads} (eV)	Configuration	G_{ads} (eV)
$6 H^+/e^-$					
6d (cont.)	* $\text{CH}_2\text{CH}_2\text{O}$		0.04	—	—
$7 H^+/e^-$					
7a	* CH_2CH		-2.54		-3.14
			-2.41		-2.60
			-2.31		-2.47
7b	* CH_3CHOH		-1.86		-1.97
			-1.55		-1.32

Table S9 The optimized adsorption configurations and adsorption free energy (G_{ads}) of the intermediates on $\text{Cu}_3\text{Zn}(111)$ and $\text{Cu}(111)$ surfaces. The solvent water molecules are not shown in snapshots. (cont.)

Label	Formula	Cu_3Zn		$\text{Cu}(111)$	
		Configuration	G_{ads} (eV)	Configuration	G_{ads} (eV)
$7 H^+/e^-$					
7c	* $\text{CH}_3\text{CH}_2\text{O}$		-2.84		-2.83
			-2.82		-2.80
			-2.71		-2.50
			-2.55	—	—
7d	* $\text{CH}_2\text{CH}_2\text{OH}$		-2.54		-2.26
			-2.53		-2.05
			-2.35	—	—
			-2.21	—	—

References

1. A. H. M. da Silva, S. J. Raaijman, C. S. Santana, J. M. Assaf, J. F. Gomes and M. T. M. Koper, *J. Electroanal. Chem.*, 2021, **880**, 114750.
2. Y. Feng, Z. Li, H. Liu, C. Dong, J. Wang, S. A. Kulinich and X. Du, *Langmuir*, 2018, **34**, 13544–13549.
3. E. Andrews, M. Ren, F. Wang, Z. Zhang, P. Sprunger, R. Kurtz and J. Flake, *J. Electrochem. Soc.*, 2013, **160**, H841–H846.
4. S. Ajmal, Y. Yang, K. Li, M. A. Tahir, Y. Liu, T. Wang, A.-U.-R. Bacha, Y. Feng, Y. Deng and L. Zhang, *J. Phys. Chem. C*, 2019, **123**, 11555–11563.
5. D. Ren, B. S.-H. Ang and B. S. Yeo, *ACS Catal.*, 2016, **6**, 8239–8247.
6. X. Su, Y. Sun, L. Jin, L. Zhang, Y. Yang, P. Kerns, B. Liu, S. Li and J. He, *Appl. Catal. B: Environ.*, 2020, **269**, 118800.
7. S. Dongare, N. Singh and H. Bhunia, *Appl. Surf. Sci.*, 2021, **556**, 149790.
8. T. Zhang, Z. Li, J. Zhang and J. Wu, *J. Catal.*, 2020, **387**, 163–169.
9. Z. Li, R. M. Yadav, L. Sun, T. Zhang, J. Zhang, P. M. Ajayan and J. Wu, *Appl. Catal. A: Gen*, 2020, **606**, 117829.
10. H. J. Monkhorst and J. D. Pack, *Phys. Rev. B*, 1976, **13**, 5188–5192.
11. T. Ludwig, J. A. Gauthier, K. S. Brown, S. Ringe, J. K. Nørskov and K. Chan, *J. Phys. Chem. C*, 2019, **123**, 5999–6009.
12. J. Santatiwongchai, K. Faungnawakij and P. Hirunsit, *ACS Cat.*, 2021, **11**, 9688–9701.
13. M. K. Sabbe, G. Canduela-Rodriguez, M.-F. Reyniers and G. B. Marin, *J. Catal.*, 2015, **330**, 406–422.
14. A. A. Peterson, F. Abild-Pedersen, F. Studt, J. Rossmeisl and J. K. Nørskov, *Energy Environ. Sci.*, 2010, **3**, 1311–1315.
15. F. Calle-Vallejo and M. T. Koper, *Angew. Chem. Int. Ed. Engl.*, 2013, **52**, 7282–7285.
16. J. K. R. Nørskov, J.; Logadottir, A.; Lindqvist, L.; Kitchin, J. R.; Bligaard, T.; Jónsson, H., *J. Phys. Chem. B*, 2004, **108**, 17886–17892.